RSC Advances

ROYAL SOCIETY OF CHEMISTRY

www.rsc.org/advances

RSC Advance

RSCPublishing

ARTICLE

Chronopotentiometric Synthesis of Quantum Dots with Efficient Surface-Derived Near-Infrared Electrochemiluminescence for Ultrasensitive Microchip-Based Ion-Selective Sensing

Cite this: DOI: 10.1039/xoxxoooooox

Received ooth January 2014,
Accepted ooth January 2014

DOI: 10.1039/xoxxoooooox

www.rsc.org/

Shengyuan Deng,[1,2] Tingting Zhang,[1] Yuan Zhang,[1] Dan Shan*,[1] and Xueji Zhang*,[1]

A novel QD with near-infrared (NIR) electrochemiluminescence (ECL) emission was prepared electrolytically by hydrodynamic chronopotentiometry, using Unithiol, a clinically-known metalantidote, as the capping agent for the fabrication of an ultrasensitive ion-selective microchip. The proposed synthetic route as well as the optical properties of QD was clarified with both morphologic and spectroscopic characterizations. In air-saturated pH 8.0 phosphate buffer with dissolved oxygen as the endogenous coreactant, an intensive NIR-ECL emission at 692 nm arose which was ascribed to the unique surface states of multidentate-chelated QDs. By tuning electrolytes, a low-potential ECL peaking at −0.79 V (vs. Ag/AgCl) could further be achieved. Based on the validated competition of heavy metallic cations to the stabilizer Unithiol as it stabilizes the aqueous dispersion of QD, the ECL emission could be significantly quenched and a home-made ECL ion-selective chip was manufactured. It was further found that capping with cation exchange membrane enabled an accelerated adsorption of metal ions and sensitized the ECL signal. Using cupric cation as a model analyte, the devised sensor showed a linear range from 10.0 pM to 1.0 mM with a detection limit down to 6.7 pM; and was successfully practised in the direct detection of Bordeaux mixture as inorganic pesticide residue on the grape skin with high accuracy and selectivity. The proposed strategy could also be extended to quantify Hg^{2+} and Pb^{2+} with stronger thiol-bonding capability than Cd^{2+}. The developed microsensing system with replicable one-step synthesis should facilitate the portable and integrated QD-based NIR-ECL applications for food hygiene inspection and environmental monitoring.

Introduction

Quantum dots (QDs) with emission in the near-infrared (NIR) window have drawn extensive interests,[1–4] especially between 650 and 900 nm as biological autofluorescence and tissue absorption are both at their minima in this region.[1,2] Recent works have indicated the advantages of NIR-emitting QDs like improved tissue penetration and reduced photochemical damage have potential applications as fluorescent labels in bioimaging and biosensing.[5–8] However, due to the intrinsic photoexcitation, the QD-based NIR photoluminescence (PL) technique still suffers from photobleaching, low quantum yield and high background noise,[9] depressing the detection sensitivity for target molecules. Therefore, seeking alternative approaches to harvest efficient NIR irradiation is of great importance.

The QD-based electrochemiluminescence (ECL) is superior to PL in terms of sensitivity and high signal-to-noise ratio due to its electro-driven nature.[10] QDs with miscellaneous functionalization have offered excellent ECL signal transduction platforms,[11] while the latest efforts were paid toward the structure-ECL relationship studies of NIR-emitting QDs and their bioanalytical applications.[12–15] For example, Ag_2Se QDs for NIR-ECL detection of dopamine,[16] and NIR-ECL immunoassays based on energy transfer from CdSeTe/CdS/ZnS QDs, double-assisted amplification of CdTe/CdS QDs and dual-stabilizer-capped CdTe probes have been reported.[17–19] Nevertheless, the current QDs-based NIR-ECL are weak and unstable, requiring complicated synthetic strategies and strong oxidants as coreactants. Thus, the main challenges for advancing NIR-ECL technology lays at fabricating efficient, replicable and facile systems.

As ECL of QDs is intrinsically susceptible to their surface states,[20,21] a surface-derived ECL by rational design of the surface-states could make a shortcut to realize NIR emission, since the surface-states of unpassivated QDs generally own narrower band-gap than the core, indicating a longer emission wavelength.[20] Multi-thiolated groups as capping agents have been reported capable of

constituting a special QD surface via tight and stable multidentate-chelation.[22–25] Inspiringly, this work utilized a clinically-known antidote agent named Unithiol or sodium 2,3-dimercapto-1-propanesulfonate (DMPS) as the stabilizer to synthesize a new kind of bidentate-chelated CdTe (DMPS-CdTe) QD through a single-step electrolysis with hydrodynamic chronopotentiometry (Scheme 1A). The produced water-soluble QDs could be uniformly spread on hydrophilic substrates with simple dip-coating due to the sulfonic functionality, which facilitated the batch fabrication of QDs modified chips. The dithiol-chelating complexes formed between multiple DMPSs and individual QD were verified resulting in unique surface states with low energy level and narrow band gap, which benefited QDs with an intensive and stable NIR-ECL emission at 692 nm only with dissolved O_2 as the endogenous coreactant. Furthermore, considering DMPS as a metalantidote in the chelation therapy against heavy metal poisoning including fatally radioactive nuclide pollonium-210,[26,27] the competitive bindings of several metal cations with DMPS would lead to a quenching effect on ECL emission (Scheme 1B). Hence, a QDs-based NIR-ECL ion-selective microchip for the detection of heavy metals was proposed (Scheme 1C).

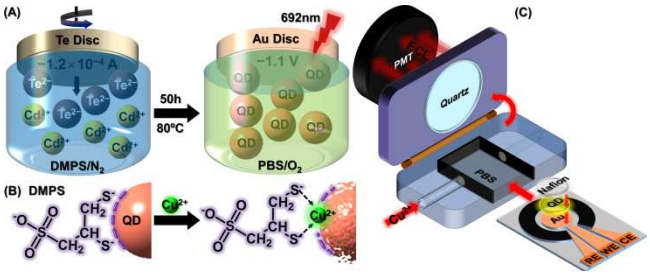

Scheme 1. (A) Schematic illustrations on one-pot synthesis of CdTe QDs with cathodic tellurium electrode in the presence of DMPS. (B) Schematic diagrams of ECL mechanism for the detection of Bordeaux mixture and (C) conceptual design of the microsensor.

Experimental

Materials and reagents

Cadmium chloride ($CdCl_2 \cdot 2.5H_2O$), Nafion-117 solution (~5% wt. in a mixture of lower aliphatic alcohols and water), DMPS, acetonitrile (≥99.9%) and tris(hydroxymethyl)aminomethane (Tris) were purchased from Sigma-Aldrich Chemical Co., Ltd. (Shanghai, China). 0.1 M acetic acid, borate, carbonate, phosphate and Tris-HNO_3 buffer salines of various pHs were prepared by mixing the stock solutions of 0.1 M corresponding buffer couple containing 0.1 M KNO_3 as the supporting electrolyte. Tellurium rod (≥99.9%, 10 mm in diameter and 10 cm in length) was purchased from Leshan Kayada Photoelectricity Co. (China) and was truncated into polytetrafluoroethylene-enclosed Te disc electrode (10 mm in the inner diameter) at the Nanjing Institute of Soil Science, Chinese Academy of Sciences. All other reagents were of analytical grade and used as received. Deionized water was implemented throughout the experiment. The O_2 or N_2-saturated solution was prepared by purging highly pure O_2 or N_2 into the solution for 30 min and preserving its atmospheric pressure. For atomic absorption spectroscopic (AAS) analysis, the skin samples of ~40 g ripe grapes were peeled and digested with the mixture of 1 M HNO_3 and 30% H_2O_2, and then neutralized with 1 M NaOH. The resulting sample solution was diluted to a constant volume prior to the instrumental measurement. For ECL detection, ~40 g ripened grapes with intact skins were immersed in 2 mL deionized water and shaken mildly at room temperature for 2 h, then 10 μL supernatant was pipetted into the detection solution.

Apparatus

UV-vis absorption spectra were recorded on a UV-3600 UV-vis-NIR spectrophotometer (Shimadzu Co., Japan). The steady-state PL and ECL spectra were collected with an Edinburgh FLS920 fluorescence spectrometer (Livingston, UK). The ECL spectrum was realized by electrolyzing the QD solution in a self-designed quartz curvette at −1.3 V upon a polished bare gold electrode (5 mm in diameter, Tianjin Aidahengsheng Technology Co., Ltd., China) via hydrodynamic potentiostatic electrolysis, *e.g.* amperometric *i*~*t* curve with a platinum wire as counter and a Ag/AgCl (saturated KCl as filling liquid) as reference electrodes. Attenuated total reflection Fourier transformation infrared (ATR-FTIR) spectra of samples on the glass slides were obtained with an IR-Prestige-21 FTIR spectrometer (Shimadzu Co., Japan). X-ray photoelectron spectra (XPS) were obtained on a K-Alpha X-ray photoelectron spectrometer (Thermo Fisher Scientific Co., U.S.A.). After vacuum coating the QDs modified screen printed electrode (SPE, 5 mm in diameter) with Au film to improve the conductivity, the morphology was observed with an XL-30E field-emission scanning electron microscope (FESEM) (Hitachi) operated at an accelerating voltage of 15 kV. The specimen was also characterized by a TECNAI-12 transmission electron microscope (TEM, Philips, UK) with an accelerating voltage of 120 kV for low-resolution and 200 kV for high-resolution TEM (HRTEM) images after drop-casting the sample dispersion onto a carbon-coated 300 mesh copper grid and dried under room temperature. The AAS detection was carried out on a Hitachi-180-80 atomic absorption spectrometer (Japan). Electrochemical experiments were performed on a CHI 760D electrochemical workstation (Shanghai Chenghua Instruments Inc., China) and ECL measurements were carried out on a MPI-EII multifunctional electrochemical and chemiluminescent analytical system (Xi'an Remex Analytical Instrument Co., Ltd., China).

Synthesis of QDs

DMPS-CdTe QDs were synthesized via the hydrodynamic chronopotentiometry and employed as the ECL nanoemitters. Typically, 5.0 mg of DMPS was dissolved by stirring in 20 mL ultrapure water containing 200 μL of 1.0 M NaOH to regulate the pH around 11. Then 120 μL of 0.1 M $CdCl_2$ was added dropwisely to achieve a homogeneous solution. Highly pure N_2 was bubbled in during the whole electrolysis procedure. The cathodic current (*I*) were applied galvanostatically at -1.2×10^{4} A upon the polished tellurium electrode. After a terminal charge quantity (*Q*) of 0.45 C was reached by setting the cathodic time (*t*) to be 3750 s, the resulting solution was airproofed in a heating bath at 80 ºC for 50 h to harvest DMPS-CdTe QDs and stored at 4 ºC prior to usage.

Micromachining of ECL sensing system

The microsensing system was divided into two parts: (1) A homemade rectangular cassette consisting of polymethyl methacrylate with a built-in flat cylindrical cavity of about 200 μL volume, a inlaid watertight O-ring and one pair of inlet/outlet for analyte flow-injection and gas ventilation (Scheme 1C). A side slit

on the microcell was reserved for the insertion of SPE. (2) SPEs modified with QDs as the microchips. A bare SPE was patterned with Adobe Illustrator CS5 in a conventional three-electrode mode consisting of a modified gold disc as working and a platinum ring as both counter and reference electrodes before committed to lithography. All potentials were quoted against this reference.

The minisized cassette can be opened and closed by a cover, and should keep closed during the ECL detection for waterproof. In practice, the entire chip was inserted into the fitted slot and put in the reserved area dented in the miniature cell with its working surface towards the transparent quartz cover for maximizing the signal collection. The ECL emission window was placed aside the photomultiplier tube (PMT, detection range: 185~850 nm) biased at –800 V with 2 times of magnification. Unless specifically mentioned, the scan rate was 100 mV s^{-1}.

Preparation of QDs modified chip

As the protic alcohols can provide the protons needed to desorb ligands on the surface of QDs with a concurrent breach of surface traps, while acetonitrile does not,[28] acetonitrile was utilized as nonsolvent instead of short-chain alcohols (*e.g.* methanol, ethanol and *iso*-propyl alcohol) during the purification of crude products. Before modification, 600 μL of the as-prepared QDs solution was purified and sedimentated in 1:2 (v/v) acetonitrile and centrifuged at 10000 *rpm* for 30 min, and then redispersed in 10 μL deionized water. The as-purified QDs could be uniformly immobilized onto the electrode surface by directly drop-casting and drying under room temperature due to the aqueous solubility of the capping agent.

Results and discussion

Characterization of DMPS-CdTe QDs

The sparsely-scattered as-purified QDs in the transmission electron microscopic (TEM) image (Fig. 1A) possess a uniform size distribution around 5 nm in diameter. The high-resolution TEM (HRTEM) image focused on individual nanocrystal with magnified local crystalline zone that was indicative of aligned CdTe lattices (Fig. 1A inset). The related energy dispersive X-ray (EDX) detection verified the existence of Cd, Te and S elements that was consistent with the XPS survey scan (data not shown). After QDs were drop-cast on the gold disk in the SPE, the scanning electron microscopic (SEM) morphology of QD membrane exhibited a homogeneous layer with aggregates less than 20 nm (Fig. 1B), which probably due to the electrostatic repulsion among the negatively charged stabilizers. This microscopic feature was desirable for coreactants access to QDs, thus improving the ECL efficiency.

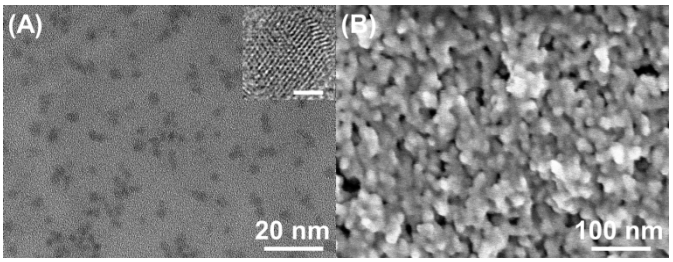

Fig. 1 (A) TEM and (B) SEM images of DMPS-CdTe QDs. Inset: HRTEM image of single QD nanocrystal (scale bar: 2 nm).

As the exciting wavelength (λ_{ex}) varied from 358 to 378 nm, the as-purified DMPS-CdTe QDs showed an excitation-independent PL behavior with an emission peak (λ_{em}) sticking around 554 nm (Fig. 2A, curve b), illustrating the typical quantum confinement with the optimal λ_{ex} $(\lambda_{ex})_{opt}$ of 368 nm (Fig. 2A, curve a). Meanwhile, it is noteworthy that there are excitation-dependent tiny peaks in the range from 400 to 450 nm. This phenomenon coincided with the fluorescence of coexisting DMPS-Te^{2-} (Fig. 2A, curve d), which was obtained by electrolyzing tellurium electrode in the alkaline DMPS solution without Cd^{2+}. These PL emissions dissipated the excitonic energy, resulting in a Stokes shift of 186 nm between $(\lambda_{ex})_{opt}$ and λ_{em}, and a nonzero tail of weak surface emission at longer wavelengths.[20] On one hand, the PL activity might reflect the relationship between the capping agent and the excitonic luminescence, suggesting that the bidentate chelation of DMPS may fabricate an uncommon surface encapsulating the core of QD. On the other hand, the PL phenomenon could be the result from incomplete passivation of the QDs surface, occurrence of surface traps, non-radiant deactivation processes, or quantum confinement effects, *etc*. Hence, to further probe this special surface chemistry as well as its embedded charge transfer kinetics, the ECL technology was employed.

Given the electro-stimulated nature, the ECL activity is much more susceptible to the surface states of QDs as compared with PL.[11,12] A broad emission peak around 692 nm was revealed in the ECL spectra from DMPS-CdTe QDs in the aqueous solution (Fig. 2A, curve c). This ECL-emitting wavelength was in the NIR region.[15,18] As an unpassivated surface of QDs usually possesses asymmetric environment like unpaired electrons, dangling bonds, ligand coordination or crystalline defects, these structural characteristics correspond a narrower valence-conduction gap than the periodically aligned core, leading to a substantially red-shifted ECL emission with respect to the PL spectrum.[20,21] This ECL NIR-emitting peak herein resulted from the electron-injected surface traps of QDs, which corresponded to the nonsymmetrical tail in the PL spectrum. Furthermore, the surface-derived NIR-ECL could be modulated by alternating the amount of DMPS moiety. As shown in Table 1, 5.0 mg of DMPS promises an efficient ECL emission with the most intensive response, indicating the obtained surface traps could facilitate the disintegration of electron/hole-injected traps and make the electron transfer between QD and the electrode easier at best.[29]

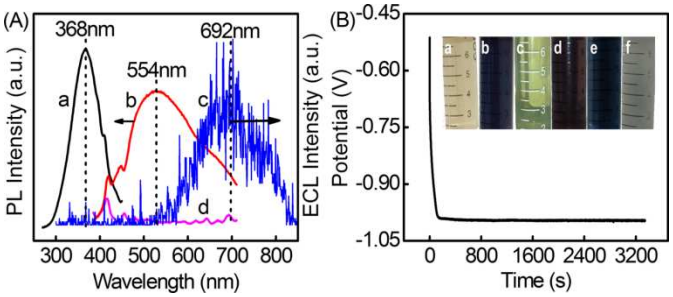

Fig. 2 (A) PL excitation (λ_{em} = 524 nm) (a) and emission (λ_{ex} = 368 nm) (b) spectra and ECL spectrum (c) of DMPS-CdTe QDs. (d) is the PL emission spectrum of DMPS-Te^{2-} in 0.1 M pH 8.0 PBS containing 0.1 M KNO_3 as the supporting electrolyte. (B) Electrochemical synthesis of DMPS-CdTe QDs via hydrodynamic chronopotentiometry. Inset: photo illustrations of the electrolyte before (a) and after (b) electrolysis, and after heating (c); (d) and (e) are the electrogenerated Te precursor with (d) and without (e) DMPS; (f) shows the color change as the introduction of Cd^{2+} into (d).

Table 1. Effect of the amount of stabilizer on ECL emission

DMPS (mg)	4.0	4.5	5.0	5.5	6.0	6.5	7.0
Normalized Peak Intensity	0.062	0.545	1.000	0.743	0.699	0.592	0.597
Peak Potential (V)	−1.45	−1.27	−1.13	−1.13	−1.12	−1.09	−1.08

Synthetic kinetics of DMPS-CdTe QDs

The Te^{2-} precursor for preparation of CdTe QDs was electrogenerated by cathodic stripping at tellurium disc electrode in the aqueous phase by a novel approach of hydrodynamic chronopotentiometry, which could easily reach the steady-state at −0.996 V after the initial plummeting in potential for 150 s (Fig. 2B). Interestingly, this electrochemical reduction was accompanied by color changes of the electrolyte from colorless to transient pink (Fig. 2B inset a) then violet (Fig. 2B inset b) and finally turned bright yellow during heating (Fig. 2B inset c). Given the equilibrium constant of 2.64 (pK_1) and 11~12 (pK_2) for H_2Te,[30] the pristine Te^{2-} basic solution presented a red wine color (Fig. 2B inset d). However, DMPS-Te^{2-} solution exhibited dark brown (Fig. 2B inset e). Considering pK_2 = 8.89 and pK_3 = 10.79 for DMPS,[30] this color contrast implied certain interaction between the ionized $-S^-$ of DMPS and Te^{2-}, whose hydrated ionic radius was larger than Cd^{2+}. The color was faded immediately by stirring after the introduction of Cd^{2+} (Fig. 2B inset f), demonstrating a more rivalrous binding between DMPS and Cd^{2+}.

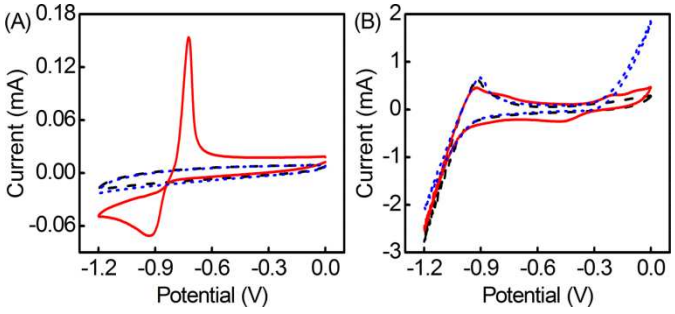

Fig. 3 Cyclic voltammograms of 12.0 μM $CdCl_2$ in 0.1 M KCl (pH 11) in the absence (solid) and presence (dashed) of 21.9 μM DMPS on (A) gold and (B) Te electrodes. Scan rate: 50 mV s^{-1}. The dotted lines were obtained in the blank electrolyte.

The potential at −0.996 V was favorable for the production of Te^{2-}, which was illustrated in Fig. 3. As the standard potential of Cd^{2+}/Cd^0 is −0.40 V (*vs*. NHS),[31] meanwhile Cd^{2+} converts into its hydroxyl complex of $[Cd(OH)_4]^{2-}$ at pH~11 with a cumulative formation constant (K_f) of 8.62,[30] the theoretic formal potential of $[Cd(OH)_4]^{2-}/Cd^0$ was calculated to be −0.87 V (*vs*. Ag/AgCl). However, due to the reduction overpotential at gold disk electrode (GDE), the cyclic voltammogram (CV) of $CdCl_2$ in 0.1 M pH 11 KCl emerged a reduction peak at −0.93 V (Fig. 3A, solid line). Upon the competitive DMPS-Cd^{2+} chelation against OH^-, the redox behavior disappeared (Fig. 3A, dashed line), indicating no electrodeposition of Cd^0 at potentials more positive than –1.2 V. On the other hand, the stripping of Te electrode into Te^{2-} produced a cathodic wave with an onset and peak potential at −0.88 and −1.2 V, respectively (Fig. 3B, solid line), which are more negative in basic media than the literature value of Te^0/HTe^- (−0.817 V *vs*. Ag/AgCl) and HTe^-/Te^{2-} (−0.794 V *vs*. Ag/AgCl).[31] The half-wave potential of −1.04 V approximates the standard value of −0.98 V in 0.1 M NaOH (*vs*. Ag/AgCl).[31] A relatively small anodic peak at −0.90 V was observed during the backward scan, indicating that a fraction of Te^{2-} was oxidized to Te^{4+}.[32] When $CdCl_2$ was introduced, its electro-reduction could also be observed at –0.49 V and vanished after the addition of DMPS (Fig. 3B, solid and dashed lines). The increase in the anodic current was considered to be the oxidation of the simultaneously formed CdTe at Te electrode surface,[32] suggesting otherwise that the CdTe species could be rapidly generated in the presence of DMPS. Therefore, the optimal applied potential for electrogeneration of Te precursor was selected at ~−1.0 V in accordance with the self-stable electrolysis at −0.996 V, which could avoid the electrodeposition of Cd. Besides, according to Sand's Equation,[33] the electrolytic reaction rate could be controlled by settling the current at -1.2×10^4 A, and the amount of Te could be dynamically adjusted based on Faraday's Law. Hence, the proposed one-pot synthetic route of CdTe QDs is a convenient, green and high replicable scheme without any demand of reductants like hydrazine,[13,17] hydroborates,[15,19] *etc*.

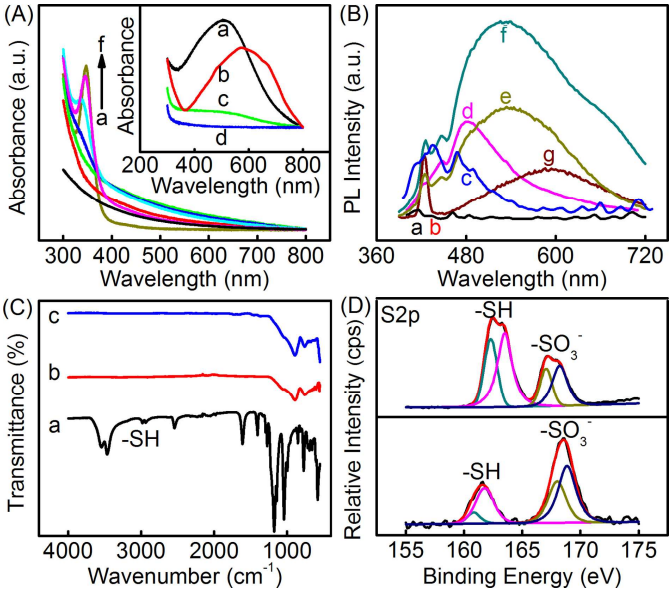

Fig. 4 (A) UV-Vis absorption spectra of DMPS-CdTe QDs obtained with different heating durations for 0, 10, 20, 30, 40, 50 and 60 h, respectively (from bottom to top), and the electrogenerated pristine Te^{2-} (a), DMPS-Te^{2-} (b) and the introduction of Cd^{2+} into (b) (c), (d) is blank solution containing DMPS as control. (B) The effect of heating time on PL emission of QDs at a sampling interval of 0 (a), 10 (b), 20 (c), 30 (d), 40 (e), 50 (f) and 60 (g) h, respectively. (C) FTIR spectra of DMPS (a), DMPS-CdTe QDs powder (b) and concentrated DMPS-Te^{2-} solution (c). (D) XPS S2p spectra of DMPS (upper) and DMPS-CdTe QDs (lower).

The obtained CdTe aqueous precursor was subsequently transferred in water bath at 80 °C to crystallize into CdTe QDs, which was monitored by UV-Vis absorption spectrum over different durations (Fig. 4A, curves a to f). As the heating proceeded from 0 to 60 h with a sampling intervel of 10 h, an inflection point at about 337 nm appeared (Fig. 4A, curve c) and gradually grew into a conspicuously symmetric absorption peak at the wavelength (λ_{ab}) of 346 nm (Fig. 4A, curve e), from which the band gap (ε_{gap}) of semiconducting nanocrystal was estimated to be 3.60 eV. The similar PL excitation (Fig. 2A, curve a) and UV-Vis absorption

wavelengths indicated that the PL emission originated from the band-gap of QD.[21] Therefore, the heating-up period was chosen to be 50 h. The relatively long time span may be a consequence of water-soluble sulfonic species as the stabilizer. Unusually, the classic Peng's empirical equation exposed its boundness when evaluating the average size of individual DMPS-CdTe QD,[34] as a positive value for calculating the dimension of CdTe QD (d_{CdTe}) requires the expression $d_{CdTe} = 9.8127\times10^{-7}\cdot\lambda_{ab}^{3} - 1.7147\times10^{-3}\cdot\lambda_{ab}^{2} + 1.0064\cdot\lambda_{ab} - 194.84 > 0$, thus λ_{ab} should be at least over 418 nm, which is inapplicable to DMPS-CdTe QD.

The above phenomena of color changes (Fig. 2B inset) were also verified by UV-Vis spectra, in which mere Te^{2-} and DMPS-Te^{2-} displayed an wide absorption peak at 512 and 573 nm, respectively (Fig. 4A, curves a and b). The absorbance of the latter diminished in solutions containing Cd^{2+} (Fig. 4A, curve c). In view of the stoichiometric ratio in micromole of [DMPS]:[Cd^{2+}]:[Te^{2-}] is 21.9:12.0:2.3, the above experiments thus demonstrated that the excessive bidentate chelators could coordinate with Te^{2-}, though the exact molecular constructure remains unclear which might refer to other known tellurium sulfides like TeS_2 and $Te[(CH_3CH_2)_2NCSS]_2$.

Instead of the UV-Vis spectra of the QDs, Fig. 4B exhibits the variation of emission spectra versus the heating time. No observable change could be witnessed within 10 h (Fig. 4B, curves a and b), implying the crystallization of QDs did not initiate yet. At 20 h, dual peaks emerged at 435 and 467 nm with a series of acromions (Fig. 4B, curve c), indicating the gradual formation of QD nucleus. The intensity of the latter peak proceeded to grow and red-shifted to 481 nm after 30 h (Fig. 4B, curve d), which further moved to 526 nm after another 10 h (Fig. 4B, curve e). At this interval, the volume of nanocrystal was augmented. According to the potential well model in quantum mechanics, the agglomeration of multiple ions thickened the electronic density of states and narrowed ε_{gap}. Further elongate the heating culminated in maximal PL intensity, *e.g.* the largest quantum yield of QDs (Fig. 4B, curve f). After that, the emission plummeted at 60 h with obvious bathochromicity as nonradiative transition prevailed in already bulky particles (Fig. 4B, curve g). The wavelength spectra have exposed interesting dynamic information.

The bidentate chelation of DMPS with the QD surface was further validated by the spectroscopic characterization of ATR-FTIR, XPS and PL spectra. Pure DMPS featured two vibrations (υ_{S-O}) at 1177.8 and 1144.1 cm^{-1} (Fig. 4C, curve a), which confirms the presence of sulfonate group.[35] Compared with DMPS, the FTIR spectra of both DMPS-CdTe QDs (Fig. 4C, curve b) and DMPS-Te^{2-} (Figure 4B, curve c) did not show the stretching modes of S−H bond at 2982.9 and 2938.5 cm^{-1},[35] indicating the dehydrogenation and their ligation of dimercaptans. Therefore, in addition to the normal metallic cations like Cd^{2+}, thiols hereby also show affinity with the electrolyzed Te^{2-} anion.

The XPS spectra of S2p were also recorded to probe the surface characteristics of QDs. The typical S2p spectrum of DMPS showed dual groups of doublet structure (Fig. 4D, upper), which was assigned to the spin-orbit splitting of –SH and $-SO_3^-$,[36] respectively, with a separation of around 4.8 eV. In comparison with the S2p spectrum of stabilizer, the corresponding $S2p_{1/2}$ and $S2p_{3/2}$ binding energies of –SH at DMPS-CdTe QDs shifted negatively from 163.5 and 162.3 eV to 161.8 and 160.9 eV, respectively (Fig. 4D, lower), with a relative intensity ratio of –SH/$-SO_3^-$ changed drastically, whereas the peak belonging to $-SO_3^-$ stand still, confirming the existence of chemical bonds between –SH of DMPS and the surface of CdTe QDs. From the above mentioned, DMPS contributed to the special surface states of QD, leading to unique optical property of surface-derived NIR ECL, of which behaviors were investigated as follows.

Electrochemical and ECL behaviors of QDs

DMPS-CdTe QDs modified SPE could be reduced in oxygen-free pH 8.0 PBS with a cathodic wave (Fig. 5A, curve a in upper inset), which could not make any cathodic ECL response (Fig. 5A, curve a). In air-saturated PBS, the CV plot showed a weak reduction peak at −0.63 V and a relatively strong reduction wave starting at −1.16 V (Fig. 5A, curve b in upper inset), which could be attributed to the electrochemically reduction of dissolved oxygen and QDs, respectively,[25] while an intensive ECL emission with the onset and peak potentials of −0.99 and −1.13 V was observed (Fig. 5A, curve b), suggesting high NIR-ECL efficiency of DMPS-CdTe QDs with only dissolved oxygen as the endogenous coreactant. Moreover, the ECL emission was quite stable in the next hundreds of cyclic sweep. As for the deaerated solution containing 320 μM H_2O_2 whose concentration approximates the saturated concentration of dissolved O_2 at room temperature under standard atmospheric pressure,[38] the ECL emission was greatly enhanced (Fig. 5A, curve d). However, in O_2-saturated PBS the ECL emission showed an intensity about twice that observed in H_2O_2 (Fig. 5A, curve e). As a consequence, O_2 was more sensitizing than H_2O_2 in the coreactant course of DMPS-CdTe QDs since it could capture more electrons from electro-reduced QDs than H_2O_2, as an observable increase in the reduction wave of O_2 emerged (Fig. 5A, curves e in upper inset), and their reaction rates were also different.[39] The negative shift of ECL peak potentials in O_2-saturated and H_2O_2-filled PBS by ~90 mV may be justified by Nernst equation with respect to the high concentration of coreactants.[31,33] In addition, the ECL intensity after the introduction of conventional coreactant $K_2S_2O_8$ with equivalent concentration could barely match for those improved by O_2 and H_2O_2 (Fig. 5A, curve c), indicating that the ready-made dissolved oxygen was the predominant and direct coreactant.

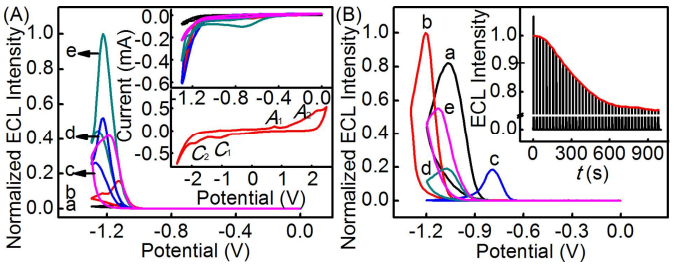

Fig. 5 (A) ECL-potential curves of QDs modified SPE in N_2-saturated (a), air-saturated (b), 320 μM $K_2S_2O_8$+N_2-saturated (c), 320 μM H_2O_2+N_2-saturated (d) and O_2-saturated (e) pH 8.0 PBS (from bottom to top). Upper inset: corresponding CVs; lower inset: CV plot of DMPS-CdTe QDs in air-free DMF containing 0.1 M TBAP. (B) ECL signals of QDs modified SPE in 0.1 M pH and electrolyte at (a) 10.0 borate, (b) 8.0 PBS, (c) 10.0 carbonate, (d) 9.5 acetic and (e) 9.0 Tris-HNO_3 buffer solutions. Inset: ECL kinetic plot after the addition of 1.0 nM Cu^{2+} into air-saturated 0.1 M pH 8.0 PBS.

As the conduction band and the valence band of an individual QD can accept (electron-injected, $QD^{\bullet-}$) and donate (hole-injected, $QD^{\bullet+}$) electrons under electrochemical conditions to produce a couple of single anion/cation radicals, an annihilation course via cyclic scan was further applied to investigate the intrinsic band parameters of

QD and its ECL mechanism.[11] To minimize the solvation effect on homogeneous CdTe QDs, the air-free dipolar aprotic solvent *N*,*N*'-dimethylformamide (DMF) was employed as the detection solution with tetrabutylammonium percholate (TBAP) as the supporting electrolyte. Dual cathodic peaks at −1.09 (C_1) and −1.90 (C_2) V and two anodic peaks at +0.76 (A_1) and +1.78 (A_2) V could be observed in the CV plot (Fig. 5A, lower inset), in which C_1 and C_2 corresponded to the reduction of unpassivated surface and bulk phase (the core) of QD, respectively:[21]

$$QD + e^- \rightarrow QD^{\bullet -} \quad [01]$$

Accordingly, A_1 and A_2 represented as each oxidized form:

$$QD - e^- \rightarrow QD^{\bullet +} \quad [02]$$

Together, the ECL emission would occur following a comproportionation reaction by radical collision or electron-hole recombination into the excited state (QD*):

$$QD^{\bullet -} + QD^{\bullet +} \rightarrow QD^* \quad [03]$$

The above electron transfer within/between the individual QD could be viewed as the formation of a non-interacting electron-hole pair, which was mediated through conduction (LUMO) and valence (HOMO) band edges.[11] The electrochemical behaviors of QDs could thus provide band information of single QD, while their potential discrepancy between the valence (−1.90 V) and conduction (+1.78 V) bands correlated to ε_{gap}, and was consistent with 3.60 eV from the optical band-gap in UV-Vis (Fig. 2A, curve f).

Meanwhile, the reduction of QD at a relatively low potential of −1.09 V indicated the DMPS-CdTe QD intrinsically possessed special surface states with low energy level, which facilitated the electron injection. In the coreactant route where coreactants interacting with QD surface, a surface-derived ECL would be favored and became dominant, because the electron transfer between the coreactant and $QD^{\bullet -}$ accelerated the formation of QD*.

In summary, this QDs-based ECL mechanism could be debriefed as the following formula: during the cathodic scan in air-saturated pH 8.0 PBS, O_2 was reduced at −0.63 V to produce oxidative intermediates like $O_2^{\bullet -}$ (Eq.[04]), $HO^{\bullet}$ (Eq.[05]) or H_2O_2 (Eq.[06]). The surface traps of DMPS-CdTe QDs served as active sites to facilitate the reactivity of QDs with coreactants (Eq.[08]) and their derivatives (Eq.[09]),[11] which reacted with electron-injected QD ($QD^{\bullet -}$)(Eq.[07]) to produce its excited state (QD*) and then gave out ECL emission (Eq.[10]). These advantages enabled the fabrication of a mild and solid-state ECL system for sensing applications.

$$O_2 + e^- \rightarrow O_2^{\bullet -} \quad [04]$$

$$O_2 + 2e^- + 2H_2O \rightarrow 2HO^{\bullet} + 2OH^- \quad [05]$$

$$O_2 + 2e^- + 2H_2O \rightarrow H_2O_2 + 2OH^- \quad [06]$$

$$nQD + ne^- \rightarrow nQD^{\bullet -} \quad [07]$$

$$O_2 + 2QD^{\bullet -} + 2H_2O \rightarrow 2QD^* + 2H_2O_2 \quad [08]$$

$$H_2O_2 + 2QD^{\bullet -} \rightarrow 2QD^* + 2OH^- \quad [09]$$

$$QD^* \rightarrow QD + h\nu \quad [10]$$

Optimization of detection parameters

Prior to the application of the proposed methodology in ECL detection of metallic cations, several experimental parameters should be optimized including the electrolytes, the solution pH and the competitive timing for cupric ion. The ECL intensity normally increased with the increasing pH value and climbed up to a maximal in each kind of buffer couples including carbonate, phosphate, borate, Tris-HNO_3 and acetic acid salts, while their normalized intensities were distinctive and peaking at various pHs (data not shown). On the other hand, as shown in Fig. 5B, the solution components also influence the ECL potential, in which a ECL peak at −0.79 V with an onset potential as low as −0.64 V could be acquired in pH 10.0 carbonate buffer (Fig. 5B, curve c). Although the peak potential of DMPS-CdTe QDs modified SPE in pH 8.0 PBS was a bit more negative, its corresponding intensity was the highest of all configurations. Meanwhile, considering the precipitation and dissolution equilibrium constant (K_{sp}) of metallic cations,[30] pH 10.0 was unfavorable for further application, thus 0.1 M pH 8.0 PBS was selected as the detection solution for the following experiments.

Quenching mechanism of QDs-based ECL by metallic cations

At room temperature, upon addition of trace Cu^{2+} (1.0×10^{-9} M) into the detection solution, the ECL intensity immediately decreased which was due to the fast diffusion of copper ions from the bulk solution to the diffusion layer.[39] The ECL kinetic curve manifested a gradually decreased intensity as time elapsed and tended to a constant quenching percentage of 26.7% after ~600 s (Fig. 5B inset), implying a complete reaction between the analyte and QDs. Therefore, the waiting time of 10 min was taken to achieve the cation exchange equilibrium. Irreversibly, the surface-derived ECL emission of QDs could not be restored to its initial intensity, indicating a permanent deterioration of surface states by Cu^{2+}. To prove the effect of this exterior corrosion, the remains of modified SPE were thoroughly rinsed with deionized water and dealt with XPS Cu2p analysis. Two spin-orbit coupling peaks of $Cu2p_{3/2}$ and $Cu2p_{1/2}$ were witnessed at 932.4 and 952.4 eV, respectively (Fig. 6A inset), which were characteristic binding section of Cu−S.[36] Thermodynamically, the K_{sp} of CuS is 6×10^{-36} lower than 8×10^{-27} of CdS.[30] In this way, a proportion of Cu^{2+} was doped into the surface of QDs. On the other side, in comparison with CdTe QDs, the relative atomic concentration of Cd element dropped from 31.92% to 17.50% after reacting with cupric ions with a similar situation for Te, suggesting the solvation of nanocrystal after the dissociation of DMPS stabilizers.

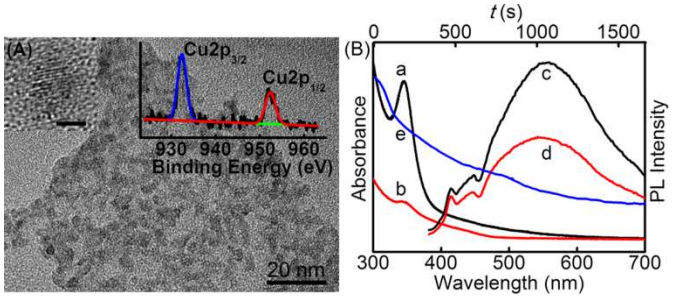

Fig. 6 (A) TEM image of QDs flocculation. Inset: HRTEM image of single QD (scale bar: 2 nm) and Cu2p XPS spectrum of QD precipitations after the addition with Cu^{2+}. (B) UV-Vis absorption (a,b) and PL emission (c,d) spectra of DMPS-CdTe QDs in air-saturated 0.1 M pH 8.0 PBS solution before (a,c) and after (b,d) the addition of 1 μM Cu^{2+} with a waiting time of 10 min. (λ_{ex} = 368 nm). (e) is the corresponding UV kinetic curve.

Since the UV and PL spectroscopies specialize in exploiting inner information of the band-gap transition, the quenching mechanism could be further clarified from the changes in UV-Vis absorption and fluorescence spectra of CdTe QDs before and after the addition of Cu^{2+}. After mixing trace amount of Cu^{2+} with QDs solution, the UV-Vis absorption peak of DMPS-CdTe QDs at 346 nm decreased drastically (Fig. 6B, curves a and b) with the UV-Vis kinetic curve (Fig. 6B, curve e) bears the resemblance with the consecutive ECL

emissions (Fig. 5B inset), indicating the electrostatic attraction between Cu^{2+} and SO_3^{2-} triggered the surface adsorption of Cu^{2+} onto QDs.. Similarly, the PL emission peak of DMPS-CdTe QDs at 554 nm also declined by 42.0%. At excessive Cu^{2+} concentrations, the gradual loss of moieties would breach the perimeter of individual QD (Fig. 6A inset) as compared with the intact one (Fig. 1A inset) and eventually culminate in flocculence, agglomeration and precipitation, which was observed in TEM images as shown in Fig. 6A.

In a word, the ECL annihilation was caused by the damage to surface states of QDs followed by the structural collapse of nanoemitters. According to the above mechanism, a disposable chip-based sensing platform is desirable for the detection of metallic ions by making use of the efficient NIR-ECL of DMPS-CdTe QDs.

Quantification of ECL sensor and analytical performance

According to the quenching effect on the cathodic ECL emission of QDs, a simple analytical strategy for the detection of Cu^{2+} was proposed. Under the optimum conditions, the ECL intensity of the developed sensor decreased with the increasing concentration of Cu^{2+} in the detection solution, during which a distorted ECL response occurred with a tiny shoulder peak around −1.13 V as a result from the large aggregation of QDs. The quenching principle follows the Stern-Volmer equation: $I_0/I = 1+K_{sv}\times c[Q]$, where I_0 and I are the initial intensity and the intensity at a given concentration of quencher c[Q], respectively, and K_{sv} is the quenching constant (Fig. 7A). The calibration plot showed a good linearity between the reciprocal of ECL intensity and the Cu^{2+} concentration in the range from 5.0 nM to 5.0 μM (R^2 = 0.997) with a detection limit of 3.8 nM at signal-to-noise of 3 (Fig. 7A inset). K_{sv} was calculated to be 6.0×10^5 M^{-1}, which is larger than 1.5×10^4 M^{-1} in CdSeTe alloyed QDs solution with *L*-cysteine as stabilizer,[40] and $1.5(4.6)\times10^5$ M^{-1} at (di)mercaptosuccinic acid-capped visible-ECL QDs at bulk electrodes,[39,41] indicating more sensitive response of DMPS-CdTe QD modified SPE to the analyte.

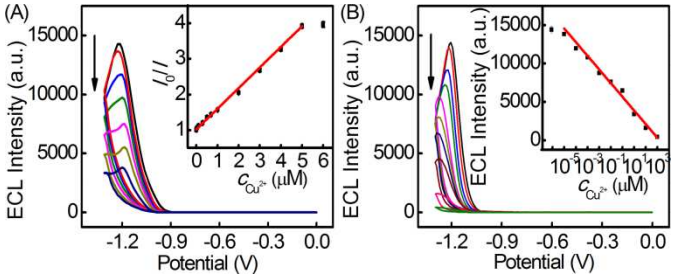

Fig. 7 Cyclic ECL curves of (A) QDs and (B) Nafion/QDs modified SPE in air-saturated 0.1 M pH 8.0 PBS in the presence of 0, 0.06, 0.5, 1.0, 2.0, 3.0, 5.0, and 7.0 μM Cu^{2+} (a−h) with a waiting time of 10 min. Insets: the corresponding linear calibration plot for Cu^{2+} detection.

To promote the performance of this chip-based ECL sensor, the cation-exchange resin of Nafion membrane was utilized to cover up QDs. The sulfonated tetrafluoroethylene-based fluoro-copolymer bears more negative charges, which facilitates the absorptive concentration of trace metallic cations, while these small ions were transported through self-organized arrays of hydrophilic water channels with ~2.5 nm in diameter by sulfonic functionalities.[42] Therefore, the modified sensor exhibited a linear relationship in a broadening detection range from 10.0 pM to 1.0 mM (R^2 = 0.992) (Fig. 7B inset). Given K_{sp} of $Cu(OH)_2$ is 1.3×10^{-20}, and $-\log K_f$ of $Cu(OH)_4^{2-}$ is 18.5,[30] no deposition was observed within this range. Interestingly, the calibration curve no longer obeys the static quenching rule based on Poisson statistics,[43] that the Cu^{2+} concentration is proportional to the ECL signal not its inverse value (Fig. 7B), indicating the change in rate determining step from a diffusion-controlled process to the ionic permeation across the membrane after the coverage of Nafion.[42] The improved ECL sensing platform thus showed a wide detection range over 9 orders of magnitude. More importantly, the detection limit was 6.7 pM (S/N=3), which was about 1000 times lower than most previously reported strategies by PL spectrometry (7.1 μM), UV-Vis (23 μM) and circular dichroism spectra (4.2 μM), graphite furnace AAS (0.1 ng L^{-1}), ion-selective electrode (98 nM), differential pulse anodic stripping voltammetry (1.41 μM) and ECL (0.9 nM).[44–49]

Interference tests

To evaluate the selectivity of our proposed sensing system, the influence of common 15 cations and 17 anions on the ECL intensity were examined. As shown in Fig. 8, the cations with strong metal(M)−S multidentate interactions (*e.g.* ML_2 or M_2L_3, L designated as DMPS) such as Ag^+, Fe^{2+} and Fe^{3+} showed slight quenching to the cathodic ECL; other ions unobviously affected on ECL emission. As expectedly, 10^{-7} M Pb^{2+}, Pd^{2+} and Hg^{2+} could largely interfere in the ECL detection of Cu^{2+} with the quenching percentage of 87.4, 95.1 and 90.4%, respectively, due to their much tighter bonding with sulfur than Cd^{2+},[30] which could also be quantified sensitively by the DMPS-CdTe QD modified SPE following the same protocol. In practice, the interfering cations could be screened with the help of halide ions by forming either water-insoluble precipitations (AgBr, $PbCl_2$, $PdCl_2$) or metal complexes (FeF_6^{3-}).[31] Although the lower K_{sp} value of HgS (4.0×10^{53}) may guarantee a sensitive response,[30] it would not impact Cu^{2+} detection, since the tolerated concentration of Hg^{2+} in real samples is usually much lower than Cu^{2+}. Thus, the as-prepared Cu^{2+} sensor had acceptable selectivity.

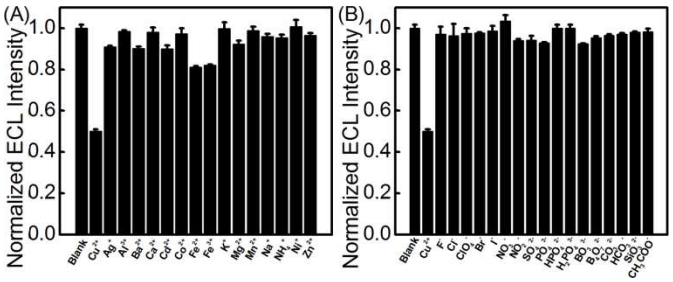

Fig. 8 Normalized ECL intensities of QD modified SPE in air-saturated 0.1 M pH 8.0 PBS in the presence of (A) 0.1 μM individual cation and (B) 0.1 μM individual anion with a waiting time of 10 min ($c[Cu^{2+}]$ = 1.0 nM).

Reproducibility, precision and analysis of real samples

The eleven ECL measurements of QDs modified SPE upon continuous cyclic scans in air-saturated pH 8.0 PBS showed coincident signals with relative standard deviation (RSD) of 1.54% (Fig. 9), indicating excellent reliability and stability of the detection signal. The ECL intensity of screen-printed QD-chips prepared with ten SPEs independently in air-saturated pH 8.0 PBS in the absence and presence of 1.0 nM Cu^{2+} showed the inter-assay RSDs of 10.3% and 8.9%, while the intra-assay of ECL ionic sensor was examined

at 1.0 nM Cu^{2+} for ten times with a RSD of 6.2%, reflecting acceptable manufacturing reproducibility and good precision. When not in use, the sensor was stored at room temperature in air condition and measured in pH 9.0 PBS daily. No obvious ECL change was observed after storage for two weeks.

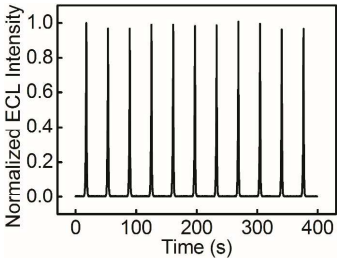

Fig. 9 Successively cyclic ECL curves of DMPS-CdTe QDs modified SPE in air-saturated 0.1 M pH 8.0 PBS.

To evaluate the analytical reliability and application potential of the proposed system, this integrated portable device was employed to detect the residue of Bordeaux mixture, a suspension of $CuSO_4$ and $Ca(OH)_2$ used as fungicide in vineyards as well as pesticide in fruit-farms and gardens.[50] Since there are news reports concerning excessive copper in red wines and underground water after applying Bordeaux mixture annually in large quantities at local plantations,[51] it is very essential to monitor and control the environmental concentration of Cu^{2+} in case it becomes a soil pollutant hazardous to fish, livestock and human beings. The result showed a copper content of 9.19±0.61 mg kg^{-1} (S/N=3) on the well-ripened grape skin, which was close to the value of 8.58 mg kg^{-1} obtained from AAS measurement. Further, when 0.1 μM standard Cu^{2+} solution was spiked into the detection solution containing the peel lixivium, the obtained recovery was 101.9±5.6% (S/N=3), indicating acceptable accuracy and practicability of the proposed method.

Conclusions

In this work, a chip-based sensing prototype for metallic ions was developed based on a novel Unithiol-capped CdTe QDs of NIR ECL emission, which was prepared via one-pot hydrodynamic chronopotentiometry with controllable and replicable conditions. This new electrolytic approach created unique surface states that Te^{2-} was convinced to chelate with DMPS like Cd^{2+}, leading to a surface-derived ECL emission at NIR wavelength. The immobilized DMPS-CdTe QDs at SPE showed efficient ECL emission in a mild condition without any exogenous coreactants. The competitive binding of Cu^{2+} to the stabilizer against Cd^{2+} enabled the remarkable ECL annihilation which was verified as a thermodynamic tendency for the formation of DMPS−Cu complex doping in QD and altered the surface states. According to this, a strategy for ultrasensitive ECL detection of Cu^{2+} was proposed, the signal of which was amplified through cation exchange, showing high sensitivity, good selectivity and stability. A house-made ion-selective chip was further manufactured for rapid detection of inorganic pesticide residue of Bordeaux mixture. The ECL NIR-emitting QDs also have the potential in versatile modifications via sulfonamide reactions and integrated into other bioassays. This work provides a facile universal route for preparing QDs with high ECL quality towards portable and disposable analytical applications.

Acknowledgements

This research was supported by National Natural Science Foundation of China (21175114, 21305067), Natural Science Foundation of Jiangsu Province (BK2011441, BK20130754), the Fundamental Research Funds for the Central Universities (30920130112012, 30920140112009), PhD Fund of MOE for Young Teachers (0133219120019), and State Key Laboratory of Analytical Chemistry for Life science (SKLACLS1302).

Notes and references

[1] *School of Environmental and Biological Engineering, Nanjing University of Science and Technology, Nanjing 210094, P.R. China. Fax: (+86) 25−8430-3107; E-mail: danshan@njust.edu.cn, drxuejizhang@gmail.com.*
[2] *State Key of Analytical Chemistry for Life Science, School of Chemistry and Chemical Engineering, Nanjing University, Nanjing 210093, P.R. China.*

1 A. M. Smith, M. C. Mancini and S. M. Nie, *Nat. Nanotechnol.* 2009, **4**, 710.
2 H. S. Choi, Y. Ashitate, J. H. Lee, S. H. Kim, A. Matsui, N. Insin, M. G. Bawendi, M. Semmler-Behnke, J. V. Frangioni and A. Tsuda, *Nat. Biotechnol.* 2010, **28**, 1300–1303.
3 L. Q. Xiong, A. J. Shuhendler and J. H. Rao, *Nat. Commun.* 2013, DOI: 10.1038/ncomms2197.
4 J. Yang, T. Ling, W. T. Wu, H. Liu, M. R. Gao, C. Ling, L. Li and X. W. Du, *Nat. Commun.* 2013, DOI: 10.1038/ncomms2637.
5 A. B. Descalzo, C. Somoza, M. C. Moreno-Bondi and G. Orellana, *Anal. Chem.* 2013, **85**, 5316.
6 Y. M. Lu, Y. Y. Su, Y. F. Zhou, J. Wang, F. Peng, Y. L. Zhong, Q. Huang, C. H. Fan and Y. He, *Biomaterials* 2013, **34**, 4302−4308.
7 G. S. Hong, J. T. Robinson, Y. J. Zhang, S. Diao, A. L. Antaris, Q. B. Wang and H. J. Dai, *Angew. Chem. Int. Ed.* 2012, **51**, 9818−9821.
8 Y. H. Chan, F. M. Ye, M. E. Gallina, X. J. Zhang, Y. H. Jin, I. C. Wu and D. T. Chiu, *J. Am. Chem. Soc.* 2012, **134**, 7309−7312.
9 R. Gill, M. Zayats and I. Willner, *Angew. Chem. Int. Ed.* 2008, **47**, 7602−7625.
10 W. J. Miao, *Chem. Rev.* 2008, **108**, 2506−2553.
11 S. Y. Deng and H. X. Ju, *Analyst* 2013, **138**, 43−61.
12 L. Sun, L. Bao, B. R. Hyun, A. C. Bartnik, Y. W. Zhong, J. C. Reed, D. W. Pang, H. D. Abruña, G. G. Malliaras and F. W. Wise, *Nano Lett.* 2009, **9**, 789−793.
13 G. X. Liang, L. L. Li, H. Y. Liu, J. R. Zhang, C. Burda and J. J. Zhu, *Chem. Commun.* 2010, **46**, 2974−2976.
14 J. Wang, X. C. Jiang, H. Y. Han and N. Li, *Electrochem. Commun.* 2011, **13**, 359−362.
15 G. D. Liang, L. P. Shen, G. Z. Zou and X. L. Zhang, *Chem. Eur. J.* 2011, **17**, 10213−10215.
16 R. Cui, Y. P. Gu, L. Bao, J. Y. Zhao, B. P. Qi, Z. L. Zhang, Z. X. Xie and D. W. Pang, *Anal. Chem.* 2012, **84**, 8932−8935.
17 L. L. Li, Y. Chen, Q. Lu, J. Ji, Y. Y. Shen, M. Xu, R. Fei, G. H. Yang, K. Zhang, J. R. Zhang and J. J. Zhu, *Sci. Rep.* **2013**, DOI: 10.1038/srep01529.
18 J. Wang, H. Y. Han, X. C. Jiang, L. Huang, L. N. Chen and N. Li, *Anal. Chem.* 2012, **84**, 4893−4899.
19 G. D. Liang,; S. F. Liu, G. Z. Zou and X. L. Zhang, *Anal. Chem.* 2012, **84**, 10645−10649.
20 N. Myung, Y. J.Bae and A. J. Bard, *Nano Lett.* 2003, **3**, 1053–1055.
21 Y. J Bae, N. Myung and A. J. Bard, *Nano Lett.* 2004, **4**, 1153–1161.
22 F. Dubois, B. Mahler, B. Dubertret, E. Doris and C. Mioskowski, *J. Am. Chem. Soc.* 2007, **129**, 482−483.
23 Y. P. Du, B. Xu, T. Fu, M. Cai, F. Li, Y. Zhang and Q. B. Wang, *J. Am. Chem. Soc.* 2010, **132**, 1470−1471.
24 C. Yuan, K. Zhang, Z. P. Zhang and S. H. Wang, *Anal. Chem.* 2012, **84**, 9792−9801.
25 X. Liu, L. X. Cheng, J. P. Lei, H. Liu and H. X. Ju, *Chem. Eur. J.* 2010, **16**, 10764−10770.
26 G. P. Guzzi and A. M. Caterina, *Toxicology* 2008, **244**, 1−12.

27 A. A. Van der Linde, S. Pillen, G. P. Gerrits and J. N. Bouwes-Bavinck, *Clin. Toxicol.* (*Phila*) 2008, **46**, 479−81.
28 A. Hassinen, I. Moreels, K. De Nolf, P. F. Smet, J. C. Martins and Z. Hens, *J. Am. Chem. Soc.* 2012, **134**, 20705−20712.
29 E. E. Lees, M. J. Gunzburg, T. L. Nguyen, G. J. Howlett, J. Rothacker, E. C. Nice, A. H. A. Clayton and P. Mulvaney, *Nano Lett.* 2008, **8**, 2883–2890.
30 Lange's Handbook of Chemistry (15th Edition): Section 8 - Electrolytes, Electromotive Force, and Chemical Equilibrium. U.S.: *New York*, 2005.
31 Lide, D. R. *CRC Handbook of Chemistry and Physics*, 88th Edition; CRC Press, Inc.: Boca Raton, *Florida*, 2008.
32 C. W. Ge, M. Xu, J. Liu, J. P. Lei and H. X. Ju, *Chem. Commun.* 2008, **4**, 450−452.
33 A. J. Bard and L. R. Faulkner, *Electrochemical Methods: Fundamentals and Applications* (Section Edition); Wiley InterScience: *New York*, 2001.
34 W. W. Yu, L. H. Qu, W. Z. Guo and X. G. Peng, *Chem. Mater.* 2003, **15**, 2854−2860.
35 W. W. Simons, *The Sadtler Handbook of Infrared Spectra*; Sadtler Research Laboratories: *Philadelphia*, 1978.
36 J. F. Mou1der, W. F. Stickle, P. E. Sobol and K. D. Bomben, *Handbook of X-ray Photoelectron Spectroscopy: A Reference Book of Standard Spectra for Identification and Interpretation of XPS Data*; Perkin-Elmer Corporation, U. S.: *Minnesota*, 1992.
37 S. H. Choi, K. Pang, K. Kim and D. G. Churchill, *Inorg. Chem.* 2007, **46**, 10564–10577.
38 H. X. Ju and H. Jiang, *Chem. Commun.* 2007, **3**, 404−406.
39 L. X. Cheng, X. Liu, J. P. Lei and H. X. Ju, *Anal. Chem.* 2010, **82**, 3359−3364.
40 G. X. Liang, H. Y. Liu, J. R. Zhang and J. J. Zhu, *Talanta* 2010, **80**, 2172−2176.
41 L. H. Zhang, L. Shang and S. J. Dong, *Electrochem. Commun.* 2008, **10**, 1452–1454.
42 K. Schmidt-Rohr, Q. Chen, *Nat. Mater.* 2008, **7**, 75−83.
43 M. A. R. B. Castanho and M. J. E. Prieto, *Biochim. Biophys. Acta* 1998, **1373**, 1−16.
44 S. H. Choi, K. Pang, K. Kim and D. G. Churchill, *Inorg. Chem.* 2007, **46**, 10564–10577.
45 A. Moletti, C. Coluccini, D. Pasini and A. Taglietti, *Dalton Trans.* 2007, 1588–1592.
46 M. Koneswaran and R. Narayanaswamy, *Sens. Actuators, B* 2009, **139**, 104–109.
47 A. M. Abdel-Lateef, R. A. Mohamed and H. H. Mahmoud, *J. Anal. Atom. Spectrom.* 2013, **3**, 8−12.
48 A. Shokrollahi, A. Abbaspour, M. Ghaedi, A. N. Haghighi, A. H. Kianfar and M. Ranjbar, *Talanta* 2011, **84**, 34−41.
49 C. M. Cheng, Y. Huang, X. Q. Tian, B. Z. Zheng, Y. Li, H. Y. Yuan, D. Xiao, S. P. Xie and M. M. F. Choi, *Anal. Chem.* 2012, **84**, 4754−4759.
50 J. W. Pscheidt and C. M. Ocamb, *Pacific Northwest Plant Disease Control Handbook* (eds. 1999); Corvallis: Oregon State University.
51 P. Pauline, *HDRA Encyclopedia of Organic Gardening* (pp. 103); Dorling Kindersley Ltd., U. K.: *London*, 2012.